American Mineralogist, Volume 80, pages 1174–1178, 1995

High-angle annular dark-field microscopy of franckeite

SU WANG,* P. R. BUSECK
Departments of Geology and Chemistry/Biochemistry, Arizona State University, Tempe, Arizona 85287, U.S.A.

J. LIU**
Center for Solid State Science, Arizona State University, Tempe, Arizona 85287, U.S.A.

ABSTRACT

Franckeite ($\sim FeSn_3Pb_5Sb_2S_{14}$) is a sulfosalt mineral with a modulated structure. Its complex composition and composite layered structure, lack of a well-defined unit cell, incommensurate character, and poor crystal quality have made its structure difficult to study by standard X-ray and electron diffraction methods. Imaging by high-angle, annular, dark-field (HAADF) scanning transmission electron microscopy provides a way of mapping compositional distributions close to an atomic scale. By comparing the structure as viewed by standard high-resolution transmission electron microscopy with the compositional information provided by the HAADF technique, we were able to test and confirm the assumption that layers consisting of multiple sheets of SnS_2 and PbS are stacked along the **a** axis with a 1.73 nm repeat.

INTRODUCTION

Franckeite has an approximate composition of $FePb_5Sn_3Sb_2S_{14}$. It is typically poorly crystalline and has a complex, composite, modulated structure (termed a layered misfit structure by Makovicky and Hyde, 1981) that has not been fully determined. A structural model was proposed by Mozgova et al. (1976) and subsequently modified by Williams and Hyde (1988) and Wang and Kuo (1991). According to the modified structural model, franckeite consists of pseudotetragonal (T) and pseudohexagonal (H) layers. The H layer has the berndtite structure (comparable to that of brucite) with composition SnS_2, in which two planes of S atoms are closely packed and most octahedral sites are occupied by Sn^{4+}. Each T layer includes two Pb-S sheets having a galena-type structure. Small amounts of Sn may be replaced by Fe^{2+} in H layers, and small amounts of Pb may be replaced by Sb^{3+} or Sn^{2+} in T layers. Negatively charged H layers alternate along **a*** with positively charged T layers, forming an HTTHTT stacking sequence that is comparable to the HTHT sequence in cylindrite (Fig. 1). The dimensional mismatch between the two types of layers results in sinusoidal modulations with a wavelength of ~4.7 nm in the **c** direction. The cell dimensions obtained from X-ray diffraction are $a = 1.72$, $b = 0.365$, and $c = 0.63$ nm for the H lattice and $a = 1.72$, $b = 0.579$, and $c = 0.582$ nm for the T lattice (Mozgova et al., 1976). The angles between axes measured from electron diffraction are $\alpha = 91.3$, $\beta = 96.2$, and $\gamma = 88.6°$ for the H lattice and $\alpha = 91.4$, $\beta = 95.5$, and $\gamma = 88.2°$ for the T lattice (Wang and Kuo, 1991).

Ambiguities in the structural model can be reconciled by using the relatively new technique of high-angle, annular, dark-field (HAADF) microscopy, which allows composition-sensitive imaging at near atomic scale using a dedicated scanning transmission electron microscope (STEM). The proposed structure of franckeite has four Pb-S atomic planes between SnS_2 layers, with interlayer spacings of ~0.29 nm. The difference between the atomic numbers of the Pb in the PbS layer and the Sn in the SnS_2 layer is sufficiently large to distinguish by HAADF. Therefore, we used the technique to test the proposed franckeite structure model.

THE STEM AND HAADF IMAGES

During the last two decades, transmission electron microscopy has become a standard mineralogical technique, and several types of instruments are in use (e.g., Buseck, 1992). Reference is commonly made to both transmission electron microscopes (TEMs) and STEMs, but the latter are a potential source of confusion because there are two distinct types of STEMs, here called dedicated STEMs and TEM-STEMs.

The two types of instruments have different optical configurations and capabilities. A TEM-STEM is simply a TEM to which scanning coils have been added. Its main imaging lenses are below the specimen plane, i.e., between the specimen and the image plane, whereas the main imaging lenses in a dedicated STEM are before the specimen. The purpose is to demagnify the electron source

* Present address: Institute of Geophysics and Planetary Physics, University of California, Riverside, California 92521, U.S.A.
** Present address: Monsanto Company, Analytical Sciences Center, 800 North Lindbergh Boulevard, U1E, Saint Louis, Missouri 63167, U.S.A.

0003–004X/95/1112–1174$02.00

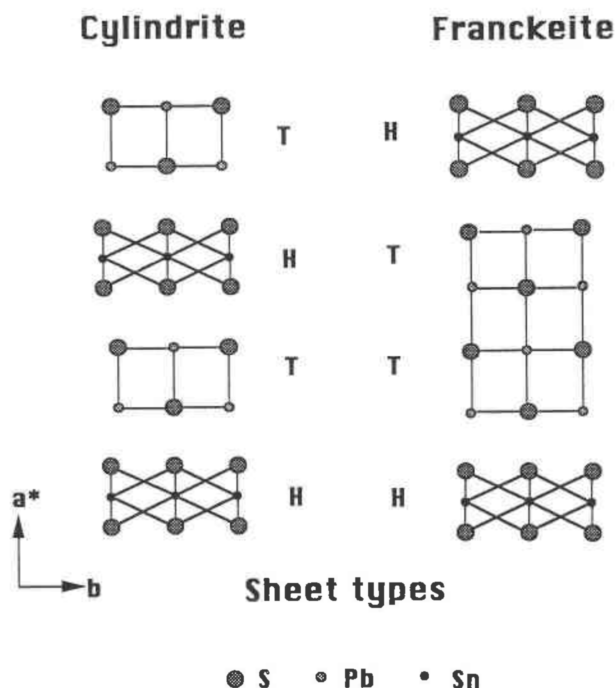

Fig. 1. Comparison of structure models of franckeite and cylindrite, idealized to be free of modulations. T = pseudotetragonal PbS layer, H = pseudohexagonal SnS_2 layer.

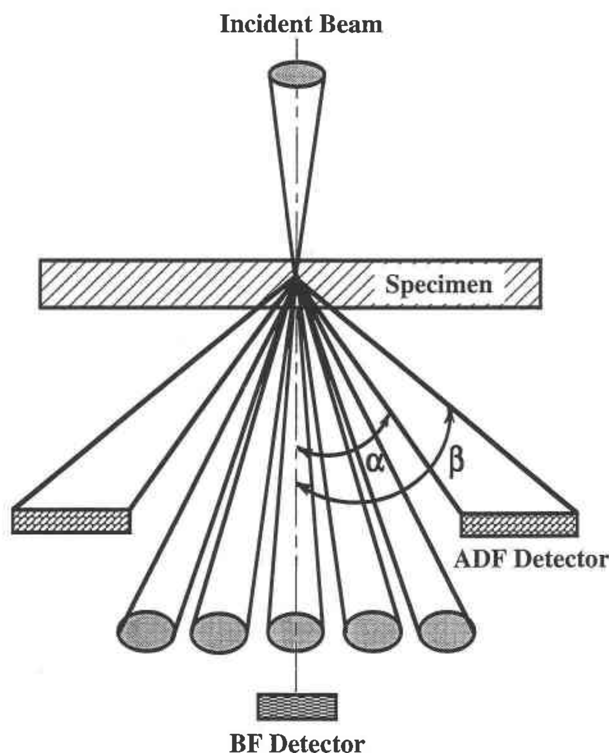

Fig. 2. Schematic diagram illustrating the annular, dark-field, detection geometry in a dedicated STEM. Inner collection angle = α, outer collection angle = β.

to form a small probe that can be scanned across the specimen. In high-resolution imaging mode, the probe diameter in a dedicated STEM is generally <0.3 nm. In standard TEM-STEMs the probe size is usually 10 nm or larger, although in new (200 kV) field-emission TEM-STEMs, a probe as small as 0.5 nm has been demonstrated, but this is still too large to resolve lattice fringes in most minerals. The probe size in our modified Vacuum Generators HB5 STEM is approximately 0.2 nm in diameter (Liu and Cowley, 1993). The optics of a dedicated STEM permit certain measurements that are difficult or impossible to make with a TEM (Cowley, 1979, 1988).

High-resolution images obtained with a TEM (or TEM-STEM) depend on the relative phases of diffracted beams, which are sensitive to sample thickness, objective lens defocus, and atomic positions and species. In contrast, use of a high-angle annular detector in STEM to form images suppresses both the phase and the diffraction effects present in conventional TEM images. The HAADF image is formed by collecting the high-angle scattered electrons with an annular detector (Fig. 2) in the diffraction plane when a small electron probe is scanned across the crystal. The image contrast is strongly dependent on the atomic number and the local thickness of the sample (Sickafus, 1988). There are no contrast reversals with beam defocus or sample thickness. At relatively thin regions of the sample and with large inner collection angles of the annular dark-field detector, the image intensity varies almost linearly with sample thickness (Liu and Cowley, 1991). If a sample has uniform thickness, a HAADF image provides a projected map that reflects the variation in average atomic weight.

For perfect single crystals, there are several contributions to the high-angle scattered signal: (1) large-angle elastic scattering (Rutherford scattering), (2) high-order Laue zone (HOLZ) Bragg reflections, and (3) thermal diffuse (multiphonon) scattering. Both experimental results and theoretical calculations have shown that the contrast of HAADF STEM images is dominated by phonon-scattered electrons (Pennycook and Jesson, 1991; Liu and Cowley, 1991; Wang and Cowley, 1989; Loane et al., 1991, 1992). The HAADF technique provides a way of mapping the compositional distributions directly with atomic resolution and has been successfully used in materials science (Pennycook and Boatner, 1988; Pennycook, 1989; Liu and Cowley, 1990, 1991).

Samples and experimental methods

Samples of franckeite were collected from the Dachang tin deposit, Guangxi, China, which was described by Huang et al. (1986). The franckeite occurs in thin tabular plates parallel to {100}. It has perfect {100} cleavage, with striations parallel to [001]. To obtain electron-transparent foils perpendicular to the cleavage planes, epoxy resin was used to glue cleavage slabs of ~1 mm thickness between two Si wafers. These "sandwiches" were fastened together and then ground and polished to a 30 μm thickness parallel or perpendicular to the striations on the

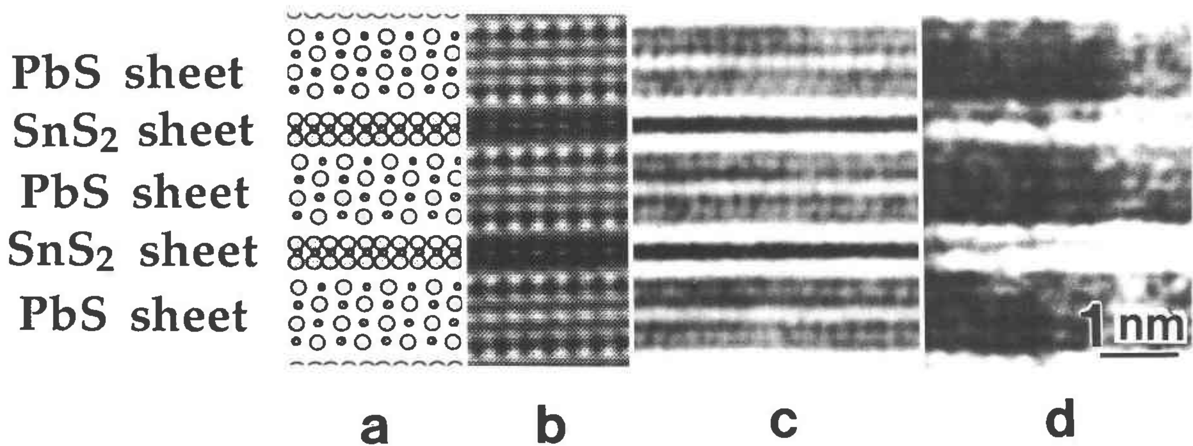

Fig. 3. (a) The [001] projection of the franckeite structure. Small circles represent metal atoms and large circles represent S atoms. (b) Simulated high-resolution TEM image. Corresponding experimental high-resolution TEM (c) and STEM (d) images. The scale bar is for all four parts of the figure.

cleavage planes. The samples were ion milled using a GATAN 600 dual ion mill with a cooling stage and examined in a modified, high-resolution, Vacuum Generators HB5 STEM operated at 100 kV. The microscope is equipped with a double-tilt, top-entry goniometer stage. The sample was also examined in a JEOL 200CX TEM operated at 200 kV with a LaB_6 filament and equipped with a ±12° double-tilt, top-entry goniometer stage.

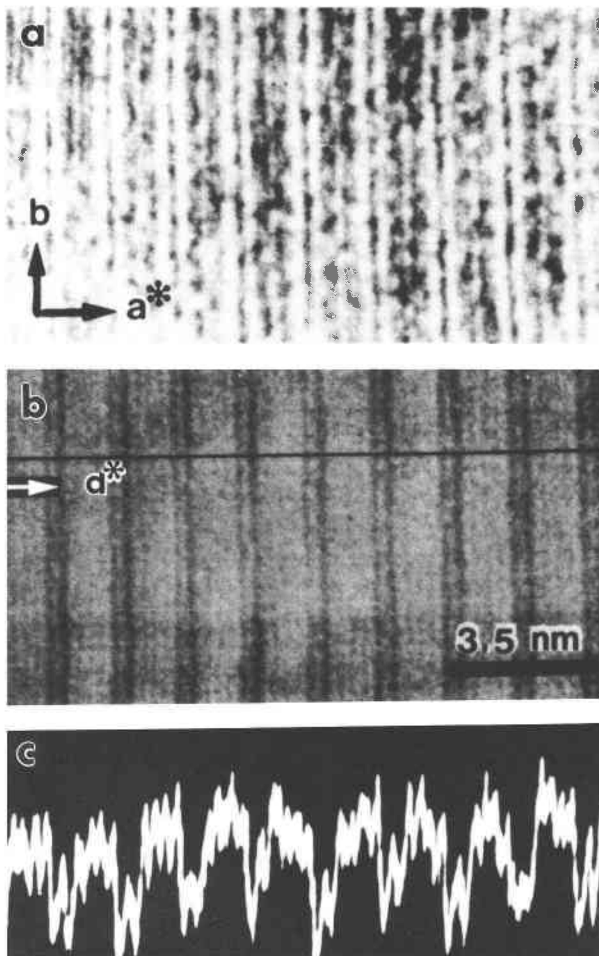

Results

Figure 3 compares the idealized structure model of franckeite to a computed image and to conventional high-resolution TEM and STEM images. The white spots in Figure 3b are aligned in rows that match the positions of low electron density in the idealized structure. These rows are also evident in the corresponding experimental TEM (Fig. 3c) and STEM (Fig. 3d) images.

A comparison between high-resolution bright-field and HAADF STEM images is given in Figure 4. Both images are from the region shown in Figure 3d but are of a larger area. The contrast in the HAADF image is inverted relative to that in the bright-field STEM image, so that the bright lines in the HAADF image occur in the positions of the atom layers. Unlike in bright-field images (TEM or STEM), the contrast in HAADF images does not change appreciably with focus.

The HAADF image contrast depends on the average atomic number of the layers (Pennycook and Boatner, 1988). The intensity distribution along the **a*** direction of the HAADF image (Fig. 4c) shows strong quadruple peaks separated by weaker single peaks. The 0.29 nm separation of neighboring peaks corresponds to the fringe

←

Fig. 4. Comparison between (**a**) a [001] high-resolution bright-field STEM image of franckeite and (**b**) a corresponding HAADF image. The broad, light bands correspond to the PbS layers, and the narrower, dark bands correspond to the SnS_2 layers. (**c**) The scan across the horizontal line (along the **a*** direction) in **b** shows the intensities of the quadrupled PbS sheets and the single SnS_2 sheets. The brighter lines indicate the positions of the sheets of heavier atoms.

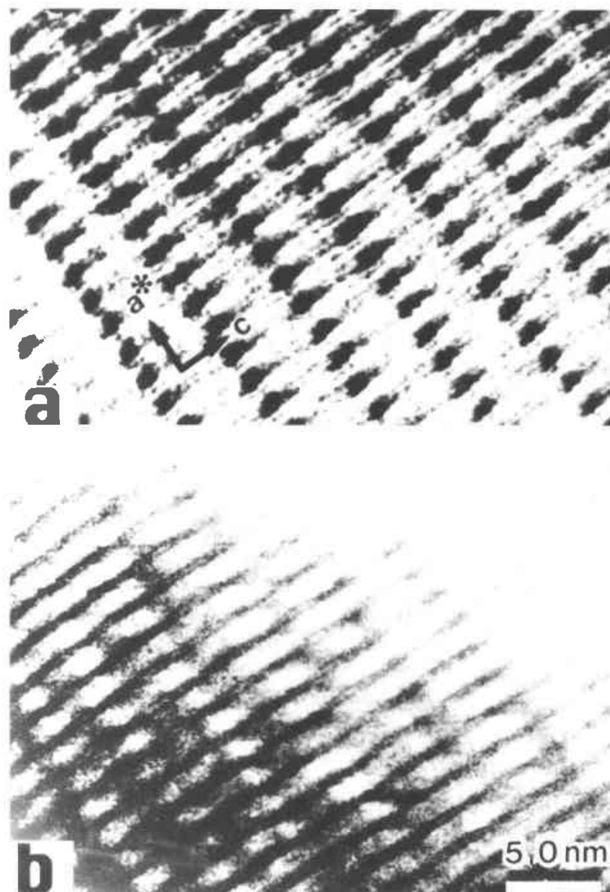

Fig. 5. (a) Franckeite [010] bright-field STEM image. (b) Corresponding HAADF image, with intensity increasing linearly with sample thickness (diagonally from lower left corner to upper right corner) (Liu and Cowley, 1991). Modulations are evident in both images. The scale bar is for both parts of the figure.

spacings (Fig. 4b). These features correspond to the structure model (Fig. 3) that contains quadrupled PbS sheets separated by SnS_2 sheets.

A question remains about the nature of the 4.7 nm modulation in the **c** direction of franckeite. We used HAADF imaging to identify the compositional contribution to the modulation. The (010) bright-field STEM image (Fig. 5a) shows a sinusoidal modulation of intensity with periodicity about 4.7 nm parallel to **c** along the sheets, similar to that observed using a TEM (Williams and Hyde, 1988; Wang and Kuo, 1991). In bright-field TEM and STEM images, however, the diffraction contrast effectively obscures any atomic number (Z) contrast that may be present and so precludes a simple chemical interpretation of the image (Rose and Gronsky, 1986). Thus, it is unclear whether a modulation in a given TEM or STEM image results from displacive (structural) or chemical effects. Such images change with defocus, no matter what the origin of the modulation. However, since HAADF images are sensitive to chemistry but are insensitive to defocus, it is possible to discern the effects of chemistry.

We imaged the same modulation with the HAADF technique as in bright-field mode with the STEM. The resultant image displays contrast variations corresponding to the sinusoidal modulation (Fig. 5b) but independent of focus conditions, showing that the modulation has a large compositional component. The significance of the 4.7 nm periodicity is related to the mismatch between the H and T sheets in the **c** direction. The compositional variation may compensate for the structural mismatch and help to form the sinusoidal modulations.

Acknowledgments

We thank E.M. Huang for providing the franckeite samples for this study and John Cowley for helpful comments. The manuscript was improved by the reviews of K.E. Sickafus, C. Moses, and G. Guthrie. Electron microscopy was performed at the Center for High Resolution Electron Microscopy (CHREM) at Arizona State University (ASU). The ASU CHREM facility is supported by the National Science Foundation (NSF) and ASU, and this research was supported by grant EAR-9219376 (to P.R.B.) from the NSF.

References cited

Buseck, P.R. (1992) Minerals and reactions at the atomic scale: Transmission electron microscopy. In Mineralogical Society of America Reviews in Mineralogy, 27, 1–36.

Cowley, J.M. (1979) Principles of image formation. In J. Hren, J.I. Goldstein, and D.C. Joy, Eds., Introduction to analytical electron microscopy, p. 1–42. Plenum, New York.

——— (1988) Imaging. In P.R. Buseck, J.M. Cowley, and L. Eyring, Eds., High-resolution transmission electron microscopy, p. 3–37. Oxford University Press, Oxford, U.K.

Huang, M., Wu, G., Chen, Y., and Tang, S. (1986) Mineralogical study of the franckeite from the Dachang cassiterite-sulphide polymetallic ore field, Guangxi. Acta Geologica Sinica, 2, 164–175.

Liu, J., and Cowley, J.M. (1990) High-angle ADF and high-resolution SE imaging of supported catalyst clusters. Ultramicroscopy, 34, 119–128.

——— (1991) Imaging with high-angle scattered electrons and secondary electrons in the STEM. Ultramicroscopy, 37, 50–71.

——— (1993) High-resolution scanning transmission electron microscopy. Ultramicroscopy, 52, 335–346.

Loane, R.F., Xu, P., and Silcox, J. (1991) Thermal vibrations in convergent-beam electron diffraction. Acta Crystallographica, A47, 267–278.

——— (1992) Incoherent imaging of zone axis crystals with ADF STEM. Ultramicroscopy, 40, 121–138.

Makovicky, E., and Hyde, B.G. (1981) Non-commensurate (misfit) layer structures. Structure and Bonding, 46, 101–170.

Mozgova, N.N., Organova, N.I., and Gorshkov, A.I. (1976) Structural resemblance between incaite and franckeite. Døklady Akademie Nauk SSR, 228, 705–708.

Pennycook, S.J. (1989) High-resolution imaging with large-angle elastically scattered electrons. Bulletin of the Electron Microscopy Society of America, 19, 67–73.

Pennycook, S.J., and Boatner, L.A. (1988) Chemically sensitive structure-imaging with a scanning transmission electron microscope. Nature, 336, 565–567.

Pennycook, S.J., and Jesson, D.E. (1990) High-resolution incoherent imaging of crystals. Physical Review Letters, 64, 938–941.

——— (1991) High-resolution Z-contrast imaging of crystals. Ultramicroscopy, 37, 14–38.

Rose, J.H., and Gronsky, R. (1986) The potential of high-resolution transmission electron microscopy for imaging impurities at dislocations and grain boundaries in silicon. Materials Research Society Symposia Proceedings, 62, 57–64.

Sickafus, K.E. (1988) Annular dark-field image interpretation in scanning

transmission electron microscopy, with application to magneto-optic recording. IBM General Products Division, Tucson, Arizona.
Wang, Su, and Kuo, K.H. (1991) Crystal lattices and crystal chemistry of cylindrite and franckeite. Acta Crystallographica, A47, 381–392.
Wang, Z.L., and Cowley, J.M. (1989) Simulating high-angle annular dark-field STEM images including inelastic thermal diffuse scattering. Ultramicroscopy, 31, 437–454.
Williams, T.B., and Hyde, B.G. (1988) Electron microscopy of cylindrite and franckeite. Physics and Chemistry of Minerals, 15, 521–544.

Manuscript received May 16, 1994
Manuscript accepted June 27, 1995